

TiO₂ treatment using ultrasonication for bubble cavitation generation and efficiency assessment of a dye-sensitized solar cell

Jae-hun Bae^a, Seong-bin Do^a, Sung-ho Cho^a, Kyung-min Lee^a, Sung-Eun Lee^{b,1}, Tae-Oh Kim^{a,c,1,*}

^a Department of Environmental Engineering, Kumoh National Institute of Technology, Gumi 39253, Republic of Korea

^b Department of Applied Biosciences, Kyungpook National University, Daegu 41566, Republic of Korea

^c Department of Energy Engineering Convergence, Kumoh National Institute of Technology, Gumi 39177, Republic of Korea

ARTICLE INFO

Keywords:

Ultrasonication
TiO₂, cavitation bubbles
Surface defects
Dye-sensitized solar cell

ABSTRACT

In this study, the impacts of different ultrasonic treatments on TiO₂ particles were determined and they were used to manufacture the photoelectrodes of a dye-sensitized solar cell (DSSC). Two methods were used to prepare TiO₂ particles directly sonicated by an ultrasonic horn, and TiO₂ treated indirectly by an ultrasonic cleaner. TEM, XPS analysis was confirmed that cavitation bubbles generated during ultrasonication resulted in defects on the surface of TiO₂ particles, and the defect induced surface activation. To understand the effect of TiO₂ surface activation on energy conversion efficiency of DSSC, ultrasonic horn DSSC and ultrasonic cleaner DSSC were prepared. The UV-vis analysis exhibited that the ultrasonic horn DSSC possessed higher dye adsorption when compared to the ultrasonic cleaner DSSC, and the EIS analysis confirmed that the electron mobility was greatly increased in the ultrasonic horn DSSC. The energy conversion efficiency of the ultrasonic horn DSSC was measured to be 3.35%, which is about 45% increase in comparison to that of the non-ultrasonic treated DSSC (2.35%). In addition to this regard, recombination resistance of ultrasonic horn DSSC was calculated to be 450 Ω·cm², increasing more than two times compared to the non-ultrasonic treated DSSC (200 Ω·cm²). Taken together, these ultrasonic treatments significantly improved the energy conversion efficiency of DSSC, which was not tried in DSSC-related research, and might lead us to develop more efficient practical route in the manufacturing of DSSC.

1. Introduction

Solar cells are clean and renewable energy sources that do not cause environmental pollution. Depending on their constituent chemicals, solar cells are divided into silicon solar cells [1,2], thin film solar cells [3,4,5], organic solar cell [6,7], dye-sensitized solar cells (DSSCs) [8,9], and perovskite solar cells [10,11]. Among them, silicon solar cells are the most commonly used because they show a high efficiency of 25% or more [1]. However, they are expensive because of their complicated manufacturing process and high energy consumption [2]. To compensate for these disadvantages, many researchers have developed new solar cells to replace silicon solar cells, and one of them is the DSSC.

The DSSC was first introduced by Grätzel in 1991. It generates electricity by irradiating light energy to a dye adsorbed on a semiconductor photoanode, and the excited electrons trigger a redox

reaction in the electrolyte [12]. TiO₂, which is a metal oxide semiconductor, is economical and has high physical and thermal stabilities, making it the most suitable photoanode for DSSCs [8,12]. Although the DSSC using TiO₂ has low cost and high stability, it has low dye adsorption and high electron recombination rates, which pose as obstacles to the efficiency improvement [9].

One of the methods of increasing the TiO₂ photoelectrode efficiency is doping with a transition metal, such as Cu [13], Zn [14], Zr, and W [15]. In our previous studies, doping with various transition metals also improved the TiO₂ efficiency. Park et al. extended the reactive region of the photoelectrode to the visible region by Cu doping and achieved a high efficiency of up to 11.35% [16]. Meanwhile, Kim et al. improved the dye adsorption by the post-treatment of Zr oxide in TiO₂ and obtained an efficiency of approximately 7.03% [17]. Lee et al. improved the specific surface area and dye adsorption by doping TiO₂ with SiO₂

* Corresponding author at: Department of Environmental Engineering, Kumoh National Institute of Technology, Gumi 39253, Republic of Korea.

E-mail address: tokim@kumoh.ac.kr (T.-O. Kim).

¹ The authors equally contributed to the paper as corresponding author.

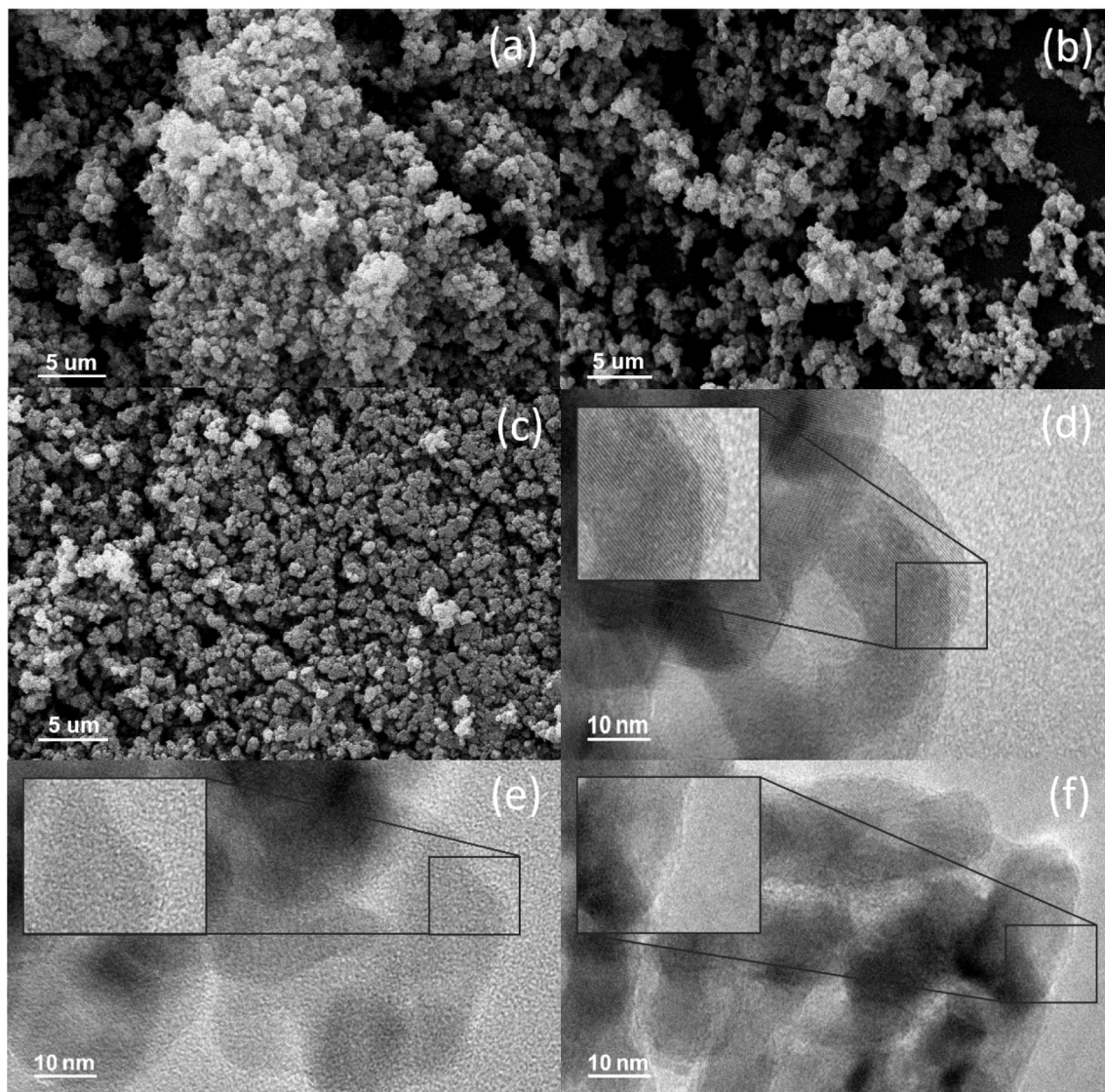


Fig. 1. (a-c) SEM images of (a) TiO₂; (b) ultrasonic cleaner-TiO₂; (c) ultrasonic horn-TiO₂. And (d-f) TEM images of (d) TiO₂; (e) ultrasonic cleaner-TiO₂; (f) ultrasonic horn-TiO₂.

and N. They enhanced the energy conversion efficiency by up to 8.68% [45]. On the contrary, current studies have encountered difficulties when adding complex heat treatment processes, such as the hydrothermal method, for doping transition metal, which consumes much time to manufacture. Therefore, a new process for improving the TiO₂ efficiency must be developed.

The methods of preparing TiO₂ into a photoanode are spin coating [18], dip coating [19], screen printing [20], and doctor blade method [20], among others. Spin coating can smoothly control the voids and thickness of the photoelectrode, but the paste may aggregate at the edges due to a centrifugal force [21]. In dip coating, the photoelectrode thickness is uniform and thin; however, as a limitation, the surface is formed non-uniformly when the paste concentration is high [22]. The screen-printing technology is advantageous for the large-scale production of paste due to uniform thickness. However, in this method, paste is thickly applied, consequently impairing the DSSC efficiency [20]. The doctor blade method is a general photoanode manufacturing method, in which TiO₂ particles are uniformly distributed inside the paste, and particle loss is small; however, when high-concentration paste is applied, the thickness is not constant, thereby needing improvement [20].

In this study, we will try to improve the energy conversion efficiency

of the DSSC by adding a simple and new “sonicated” process to the currently used doctor blade preparation method. Sonication is one of the processes used to form nanoparticles. It leads to surface activation by forming defects on the particle surface as a cavitation reaction [23,24,25]. The cavitation reaction is defined as a process in which bubbles in a fluid are formed, grown, and collapsed [26,27]. It was confirmed that the cavitation reaction is a physical and chemical reaction that oxidizes and activates the catalyst surface [28,29,30]. Hafeez et al. reported that the high heat and pressure accompanying the cavitation reaction cause defects and deformation on the particle surface, which contribute to the catalyst activation [23]. Narakaew attempted to improve the activation and reactivity of the TiO₂ surface by the cavitation phenomenon [36]. In addition, Stucchi et al. improved the dispersion of the active area by dispersing the particles through ultrasonication [35,36]. Thus, ultrasonic treatment could result in surface activation and improves the performance of catalysts and photocatalysts by uniformly dispersing materials. However, the sonication process has rarely been applied in the DSSC studies reported so far. Therefore, in the present study, a DSSC was manufactured by applying ultrasonicated TiO₂ to the photoelectrode. Its applicability and superiority are then investigated. The effect of TiO₂ treated with ultrasonic cleaner and ultrasonic horn on the DSSC efficiency is also studied.

Table 1

Comparison of Brunauer-Emmett-Teller (BET) characteristics of each TiO_2 .

Samples	Textural analysis S_{BET} (m^2/g)
TiO_2	87.5003
Ultrasonic cleaner- TiO_2	88.1523
Ultrasonic horn- TiO_2	87.4388

2. Experimental

2.1. Materials

The DSSC used in this experiment was prepared using TiO_2 (anatase 99.9%, US Research Nanomaterials, Houston, TX), α -terpineol (98.5%, Samchun Chemicals, Seoul, South Korea), chloroplatinic acid hydrate (Sigma Aldrich, St. Louis, MO), N719 dye (Solaronix, Aubonne, Swiss), ethanol (HPLC grade, Duksan Co., Ansan, South Korea), and ethyl cellulose 10 cP (extra pure, Daejung Chemicals & Metals, Siheung, South Korea). An ultrasonic cleaner (JAC2010, KODO Technical Research Co., Hwasung-si, South Korea) and an ultrasonic horn (VC750, Sonics & Materials, Newtown, CT) were used as the ultrasonic treatment equipment.

2.1.1. Preparation of the TiO_2 (commercial TiO_2) paste

The TiO_2 paste was prepared through the sol-gel method with 25 ml ethanol, 2.15 ml α -terpinol, and 0.6 ml distilled water added to 2 g of TiO_2 and stirred at 120 °C at 300 rpm for 15 min. Subsequently, 0.3 g of ethyl cellulose was added and stirred until the paste was completed. The complete paste was applied to the FTO plate by the doctor blade method, which is a method of coating with a constant thickness using a blade, and the process is as follows. In order to prepare a photoelectrode having an area of 5 mm × 5 mm on FTO glass, the other areas were masked. After this process, a certain amount of paste was repeatedly coated on glasses with 5 to 10 times using a blade, and the TiO_2 photoelectrode was manufactured by a calcination process at 450 °C for 2 h at a temperature increase rate of 5 °C/min. The photoelectrodes were immersed in an N719 dye (0.5 mM) in ethanol at room temperature for 24 h.

2.1.2. Preparation of the ultrasonic cleaner- TiO_2 paste

The ultrasonic cleaner- TiO_2 paste manufacturing added an indirect ultrasonic treatment process to the same method for the TiO_2 paste preparation. After adding 2 g of TiO_2 to 50 ml of ethanol, ultrasonic treatment (intensity high) was indirectly performed in an ultrasonic cleaner bath for 30 min to prepare an ultrasonic cleaner- TiO_2 solution. α -Terpinol (2.15 ml) and 0.6 ml distilled water were added to the ultrasonic cleaner- TiO_2 solution and stirred at 120 °C at 300 rpm for 15 min. After this process, 0.3 g ethyl cellulose was added and stirred until the paste was completed. An ultrasonic cleaner- TiO_2 photoelectrode was then manufactured in the same manner as that of TiO_2 .

2.1.3. Manufacture of the ultrasonic horn- TiO_2 paste

The ultrasonic horn- TiO_2 paste was manufactured in the same manner as the ultrasonic cleaner- TiO_2 paste. Ultrasonic treatment was directly performed. An ultrasonic horn- TiO_2 solution was prepared by directly sonicating a solution, in which 2 g of TiO_2 was added to 50 ml of ethanol with an ultrasonic horn for 30 min. Thereafter, an ultrasonic horn- TiO_2 photoelectrode was manufactured in the same manner as the ultrasonic cleaner- TiO_2 .

2.1.4. Counter electrode manufacturing and joining

The counter electrode was ultrasonically cleaned in ethanol for 15 min after drilling two holes through which the electrolytes could be injected in the FTO glass. A H_2PtCl_6 solution was coated on the washed FTO glass by spin coating and then calcined at 350 °C for 1 h to prepare a counter electrode. After joining the prepared counter electrode and the photoanode, Iodolyte AN-50 was injected as an electrolyte, and the hole was closed to complete the DSSC.

2.2. Characterization

The scanning electron microscopy (SEM, $\times 3000$), transmission electron microscopy (TEM, $\times 250000$), Brunauer-Emmett-Teller (BET), and X-ray diffraction (XRD, scan rate 5°/min), and X-ray photoelectron spectroscopy (XPS) analyses were performed in powder form. XRD and XPS were performed to understand the shape and structure of the manufactured TiO_2 . The specific surface area was measured through BET. The surface properties were analyzed through SEM and TEM analyses. The prepared DSSC was analyzed with photo-electrochemical

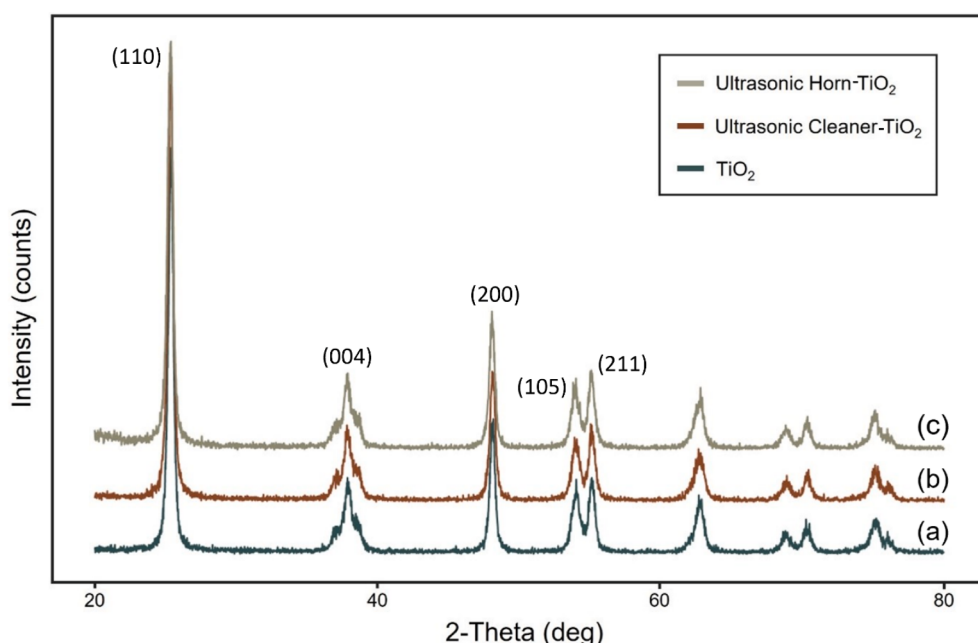


Fig. 2. XRD patterns of (a) TiO_2 ; (b) ultrasonic cleaner- TiO_2 ; (c) ultrasonic horn- TiO_2 .

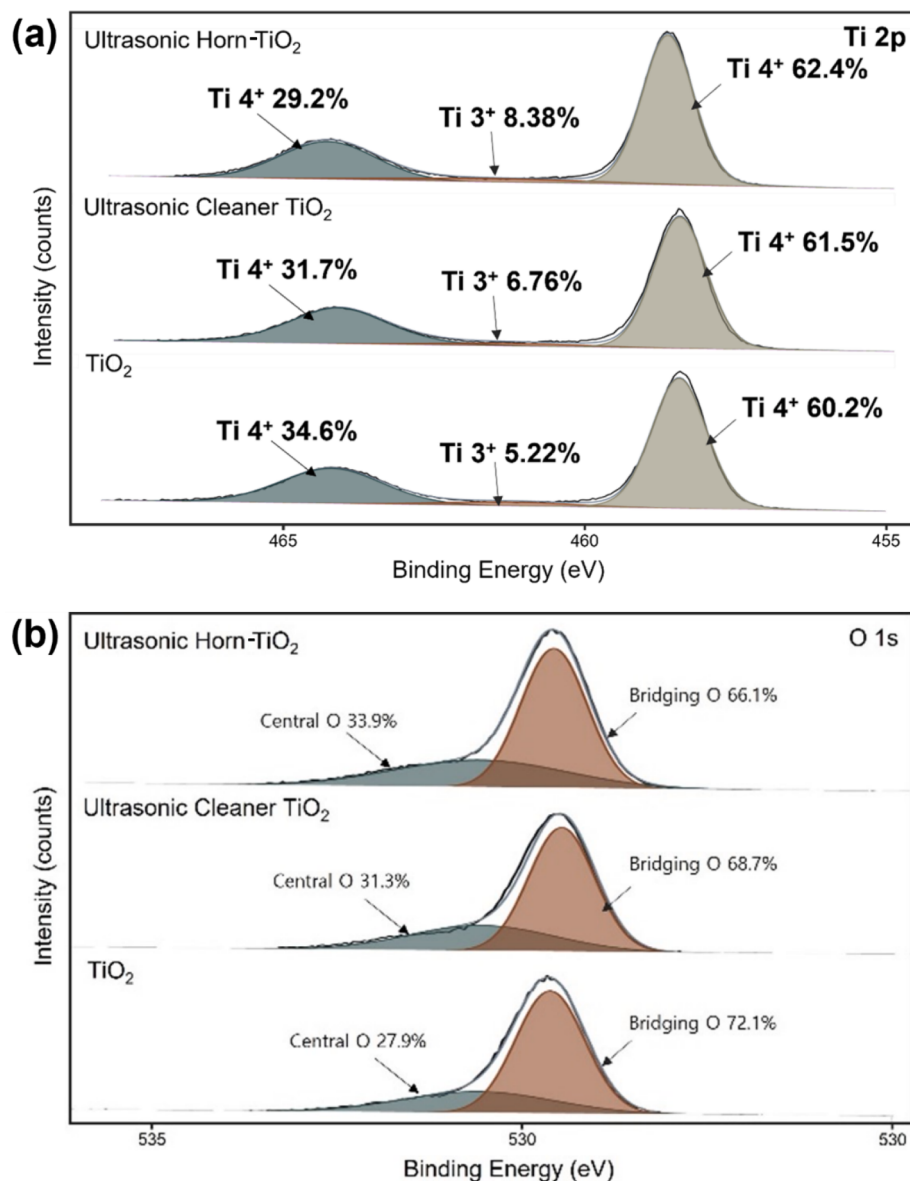


Fig. 3. (a) XPS survey spectrum Ti 2p of TiO₂, ultrasonic cleaner-TiO₂, ultrasonic horn-TiO₂; (b) XPS survey spectrum O 1 s of TiO₂, ultrasonic cleaner-TiO₂, ultrasonic horn-TiO₂.

data using 2400 source (Keithley Instruments) under AM 1.5 illumination (100 mW/cm²). The electron mobility of the electrode was analyzed by EIS. The chemical capacitance and the recombination resistance were calculated using the EIS and efficiency data.

3. Results and discussion

3.1. Characteristics analysis of TiO₂

The SEM analysis was performed to determine the dispersion of TiO₂, ultrasonic cleaner-TiO₂, and ultrasonic horn-TiO₂ (Fig. 1). The particles in TiO₂ (Fig. 1 a) were agglomerated, whereas those in the ultrasonically treated ultrasonic cleaner-TiO₂ and ultrasonic horn-TiO₂ were dispersed (Fig. 1 b and c). The dispersion degree of the directly applied ultrasonic horn-TiO₂ was relatively higher than that of the indirectly applied ultrasonic cleaner-TiO₂, which was consistent with the results of the previous studies showing that ultrasonic waves affect the particle dispersion [36]. The BET analysis was performed to determine the change in the specific surface area before and after the sonication of

each TiO₂ (Table 1). The specific surface areas were measured to be approximately 87.50 m²/g for TiO₂, approximately 88.15 m²/g for ultrasonic cleaner-TiO₂, and approximately 87.44 m²/g for ultrasonic horn-TiO₂. Although the ultrasonic waves affected the particle dispersion, they were thought to not contribute to the changes in the specific surface area.

The previous analysis showed the external change of the TiO₂ particles by ultrasonication. The changes in the properties of the inside of the particles were confirmed by the results of the TEM, XRD, and XPS analyses. Fig. 1 (e-h) depict the TEM images of each sample measured at 250,000 × magnification. Accordingly, TiO₂ particles with a diameter ranging from 30 nm to 50 nm were observed. The roughness of the outside of the particle was increased by the ultrasonication, which is more clearly shown in the insets describing TiO₂ (Fig. 1 e) and ultrasonic horn-TiO₂ (Fig. 1 f). It was assumed that the ultrasonic wave was applied to the liquid medium (ethanol) mixed with TiO₂, and the generated cavitation bubble formed a defect on the particle surface. The TiO₂ surface defects occurred in the form of an oxygen vacancy or Ti³⁺ [31,32] and did not significantly affect the surface area of the particle

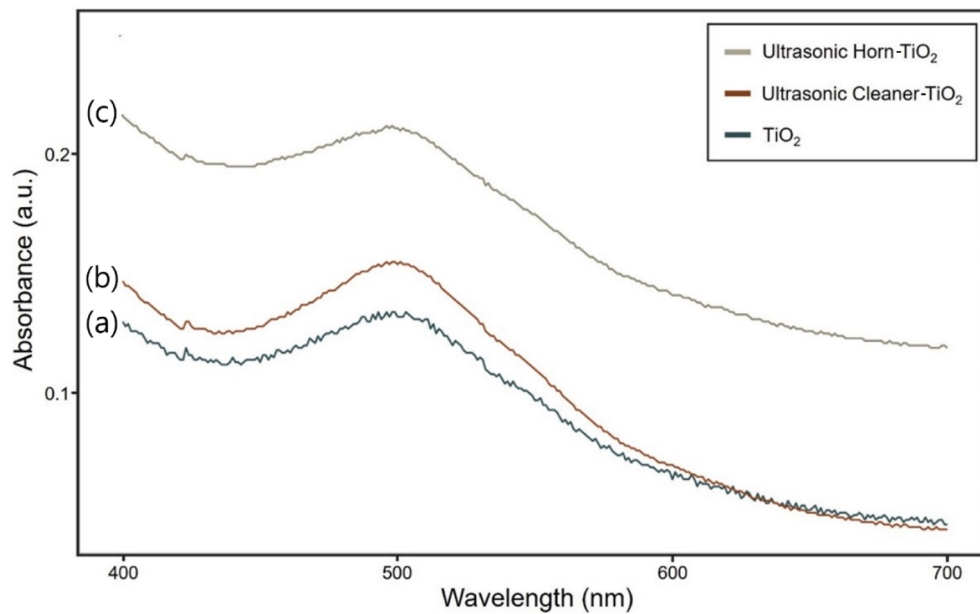


Fig. 4. UV-visible absorption spectrum for the dye adsorption assessment. (a) TiO_2 ; (b) ultrasonic cleaner- TiO_2 ; (c) ultrasonic horn- TiO_2 .

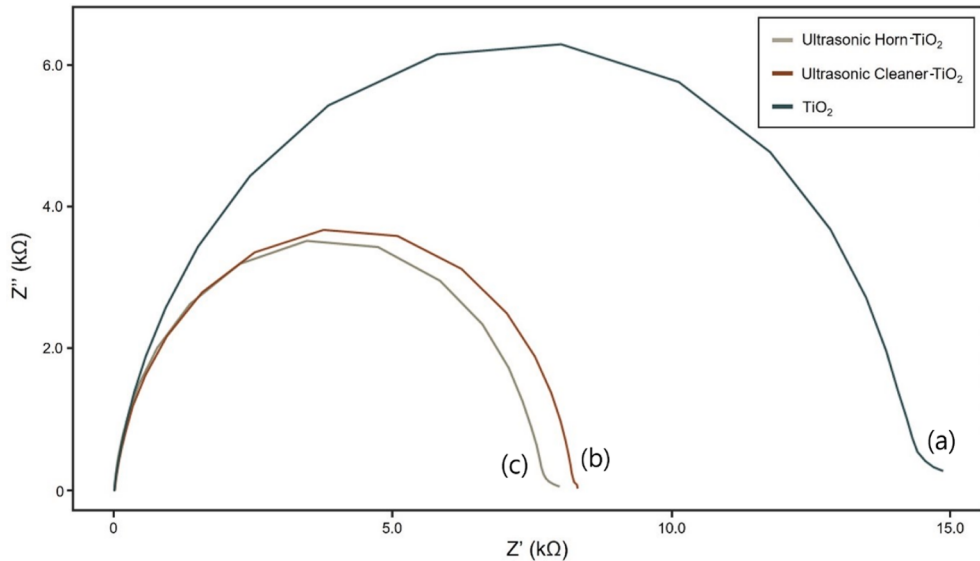


Fig. 5. EIS Nyquist plot (under dark condition) of (a) TiO_2 ; (b) ultrasonic cleaner- TiO_2 ; (c) ultrasonic horn- TiO_2 .

itself. It may, however, contribute to the particle surface activation [33]. This is related to the XPS analysis results, which will be described later. The TiO_2 surface activation caused by the defects improved the photocatalytic performance [34].

Fig. 2 shows the XRD analysis results comparing the ultrasonic cleaner/ultrasonic horn- TiO_2 and TiO_2 . Three spectra with almost identical diffraction peaks were identified, regardless of ultrasonication. The distinct diffraction peaks at 25°, 38°, 48°, 54°, and 55° were consistent with the intrinsic spectrum of the anatase phase TiO_2 (JCPDS no.: 88-1175 and 84-1286) [37,38]. This indicates that no change occurred in the crystal compositions of the three TiO_2 used herein.

The XPS analysis was performed to analyze the oxidation state of each TiO_2 surface. Fig. 3 depicts the obtained results. All XPS analyses were corrected for C 1 s (284.6 eV). In the Ti 2p spectrum, two peaks corresponding to Ti^{4+} (i.e., Ti^{4+} 2p_{1/2} and Ti^{4+} 2p_{3/2}) and one peak representing Ti^{3+} (i.e., Ti^{3+} 2p_{1/2}) were analyzed. The Ti^{3+} 2p_{1/2} peak originated from the oxygen vacancy on the TiO_2 surface caused by

ultrasonication, indicating that the ultrasonic wave activated the TiO_2 surface [39,40]. The proportion of Ti^{3+} on each TiO_2 surface was the highest in the ultrasonic horn- TiO_2 (8.38%). Those of the ultrasonic cleaner- TiO_2 and TiO_2 were 6.76% and 5.22%, respectively. These results demonstrate that ultrasonic treatment induced the TiO_2 surface activation.

The O 1 s spectrum showed the oxygen species present on the TiO_2 surface. The peaks corresponding to the lattice oxygen (bridging O, 529–530 eV) and active oxygen (central O, 530–532 eV) of TiO_2 were found in the O 1 s spectrum [41–43]. As shown in Fig. 3, the active oxygen in the ultrasonic horn- TiO_2 was 33.96%; that in the ultrasonic cleaner- TiO_2 was 31.27%; and that in C- TiO_2 was 27.89%. These results were consistent with those of the Ti 2p spectrum, in which the ultrasonic treatment improved the active oxygen content of TiO_2 and activated the TiO_2 surface.

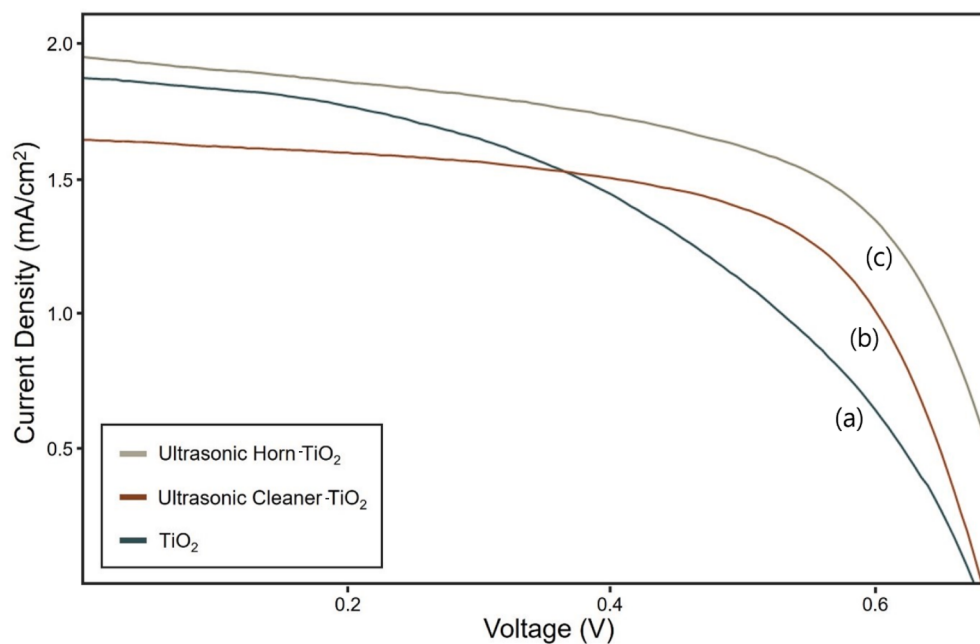


Fig. 6. Photocurrent density–voltage (J-V) graph of the DSSCs (under one-sun illumination of 1000 mW/cm^2). (a) TiO_2 ; (b) ultrasonic cleaner- TiO_2 ; (c) ultrasonic horn- TiO_2 .

Table 2

Summary of energy conversion efficiency of the DSSCs according to sonication.

Samples	J_{sc} (mA/cm^2)	V_{oc} (V)	FF (%)	η (%)
TiO_2	5.54	0.68	45.8	2.35
Ultrasonic cleaner- TiO_2	6.40	0.68	64.5	2.82
Ultrasonic horn- TiO_2	7.47	0.72	62.3	3.35

Table 3

Parameters for calculating the chemical capacitance and the recombination resistance. ΔE_c means the difference in conduction band energy (E_c) between each material. Since these samples have the same chemical composition, there is no change in the E_c value.

Samples	ΔE_c	j_0 (mA/cm^2)	R_0 ($\Omega \text{ cm}^2$)	R_s ($\text{k}\Omega$)
TiO_2	Ref.	5.54×10^{-3}	3.81×10^6	43.46
Ultrasonic cleaner- TiO_2	0	6.40×10^{-3}	4.54×10^6	26.88
Ultrasonic horn- TiO_2	0	7.50×10^{-3}	8.30×10^6	25.12

3.2. Characteristics analysis of DSSC

The previous analysis results confirmed that ultrasonic treatment activates the TiO_2 surface. UV-vis, EIS, J-V graph analyses were employed to prove how the surface activation of TiO_2 affected the DSSC efficiency. First, the ultraviolet-visible (UV-vis) spectrum was used to check the dye adsorption, which was the main electron source of the DSSC herein, to confirm the increase in the dye adsorption (Fig. 4). To evaluate the amount of dye adsorption, the absorbance was measured by adsorbing dye to the photoelectrode for 24 h, then desorbing it with 1 mM KOH solution [44]. At 500 nm wavelength, the absorbance of the ultrasonic horn was significantly higher than that of the other two samples. The amount of dye adsorbed on the photoelectrode surface was observed in the following order: ultrasonic horn- TiO_2 > ultrasonic cleaner- TiO_2 > TiO_2 .

When compared to other two treatments, the ultrasonic horn- TiO_2 exhibited a higher dye adsorption caused by the particle surface activation, which was due to the cavitation bubbles with particle dispersion [45]. The high dye adsorption of the ultrasonic cleaner- TiO_2 and the ultrasonic horn- TiO_2 acted as a key factor for improving the energy conversion efficiency of the DSSC by increasing the current density

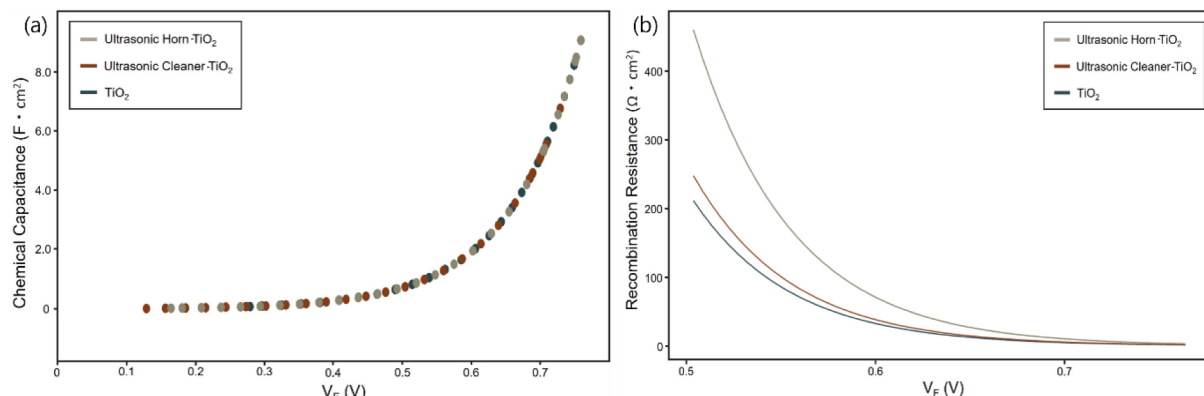


Fig. 7. Graphs for the (a) chemical capacitance and the (b) recombination resistance of TiO_2 , ultrasonic cleaner- TiO_2 , ultrasonic horn- TiO_2 .

[46,47].

Through the EIS analysis, impedance was measured to determine the electron transfer resistance. Fig. 5 depicts the EIS data observed under dark conditions. The semicircle in Fig. 5 depicts the charge transfer resistance measured at approximately 15 kΩ, with TiO₂ being the highest. The semicircle size of the ultrasonic cleaner-TiO₂ and the ultrasonic horn-TiO₂ was approximately 7–8 kΩ, confirming that the charge transfer resistance was 50% lower than that of TiO₂. The resistance received by the electrons was low when the charge transfer resistance was low; thus, the current flowed well and may act as a factor for improving the DSSC efficiency.

The energy conversion efficiency of each TiO₂ photoanode was evaluated. Fig. 6 shows the J-V graph measuring the energy conversion efficiency. Table 2 lists the parameters. The energy conversion efficiency of the ultrasonic cleaner-TiO₂ was 2.82%, which improved by approximately 20% compared to TiO₂ (2.35%). The ultrasonic horn-TiO₂ showed an efficiency of 3.35%, which was 43% higher than that of TiO₂ (2.35%) and approximately 19% higher than that of the ultrasonic cleaner-TiO₂. The amount of dye adsorption was increased by the dispersion effect of ultrasonication and the activation effect of the TiO₂ surface, which increased the current density. In conclusion, sonication contributed to the increase of the DSSC efficiency by lowering the electron transfer resistance and increasing the current density.

The chemical capacitance (C_μ) and the recombination resistance (R_r) were calculated to confirm the electrical characteristics of the DSSCs prepared using TiO₂ as a photoelectrode. The two calculations were based on the method proposed by Bisquert and the results of our previous study [44,48,49,50]. Table 3 shows the parameters required for the calculation. In the table, ΔE_c denotes the difference in E_c between each TiO₂. We found no change in the E_c value because the materials were chemically identical to each other. The R_0 value is a parameter that determines the effect on the recombination process (Eq. (4)). The R_s value indicates the series resistance of the DSSC and obtained herein using the EIS data.

$$C_\mu = L(1-p)qg(E_{Fn}) \quad (1)$$

In Eq. (1), L denotes the TiO₂ film thickness; p denotes the photoelectrode porosity; and q denotes the elementary charge.

$$g(E_{Fn}) = \frac{\alpha q N_L}{k_B T} \exp[\alpha(E_{Fn} - E_c)/k_B T] \quad (2)$$

Eq. (2) presents the Fermi level (E_{Fn}), Boltzmann constant (k_B), total density of the bandgap states (N_L), and exponent of the electrons below the conduction band. It is calculated using the constant (α) for the parameter for the exponential trap distribution of electrons under the conduction band.

$$R_r = R_0 \exp\left[-\beta \frac{qV_F}{k_B T}\right] \quad (3)$$

The recombination resistance (R_r) is calculated using Eq. (3). The variable V_F (Fermi level voltage) important for the R_r calculation is calculated using Eq. (5). V_{appl} represents the applied voltage.

$$R_0 = \frac{k_B T}{\beta q J_{sc}} \exp\left[\frac{\beta q V_{oc}}{k_B T}\right] \quad (4)$$

$$V_{appl} = V_F - jR_s \quad (5)$$

$$V_{ecb} = V_F - \Delta E_c / q \quad (6)$$

The equivalent common conduction band voltage (V_{ecb}) of the V_F value had the same value as the V_F because the material used for each TiO₂ photoanode is chemically the same. Therefore, the chemical capacitance and the recombination resistance data using V_{ecb} were not presented herein.

The chemical capacitance in Fig. 7(a) showed similar C_μ values because each DSSC applied to the calculation is chemically the same

material. Meanwhile, the recombination resistance in Fig. 7(b) illustrated values of approximately 200 Ω cm² for TiO₂ and approximately 450 Ω·cm² for ultrasonic horn-TiO₂ at V_F 0.5 V. The R_r values increased more than twice because the open-circuit voltage was increased by the effect of the ultrasonic treatment. The increase in the recombination resistance was one of the factors that increased the energy conversion efficiency along with the increases of the dye adsorption and the current density.

4. Conclusions

In this study, a TiO₂ photoelectrode was fabricated through a simple ultrasonication treatment. The surface area change of TiO₂ was analyzed by performing SEM and TEM analyses. Ultrasonic treatment greatly improved the particle dispersion and activated the TiO₂ surface. The XRD analysis confirmed that the anatase structure was maintained, even after ultrasonic treatment. The structural TiO₂ surface activation was analyzed by XPS, and the results showed that the cavitation bubble increased the active area of TiO₂. The effect of the TiO₂ surface activation on the DSSC efficiency was investigated through UV-vis and EIS analyses. The UV-vis analysis revealed that sonication significantly increased the dye adsorption. Meanwhile, the EIS analysis confirmed that sonication reduced the charge transfer resistance. Although the chemical capacitance of each TiO₂ was calculated, the materials used in each DSSC were chemically identical, showing similar capacities. The measurement of the energy conversion efficiency of the DSSC depicted that the DSSC consisting of ultrasonic horn-TiO₂ had an energy conversion efficiency of 3.35%, displaying approximately 45% of improvement compared to TiO₂ (2.35%). In addition, the recombination resistance was calculated using the open-circuit voltage and current density values of the DSSC. The results confirmed that ultrasonic treatment contributed to efficiency improvement by increasing the recombination resistance. In conclusion, the simple and effective sonication described in this paper will be very helpful in improving the DSSC efficiency.

Declaration of Competing Interest

The authors declare that they have no known competing financial interests or personal relationships that could have appeared to influence the work reported in this paper.

Acknowledgements

This research was supported by Kumoh National Institute of Technology (202001120001).

References

- [1] M.A. Green, The path to 25% silicon solar cell efficiency: History of silicon cell evolution, Prog. Photovoltaics Res. Appl. 17 (3) (2009) 183–189, <https://doi.org/10.1002/pip.v17.3.10.1002/pip.892>.
- [2] T.M. Razýkov, C.S. Ferekides, D. Morel, E. Stefanakos, H.S. Ullal, H.M. Upadhyaya, Solar photovoltaic electricity: Current status and future prospects, Sol. Energy 85 (8) (2011) 1580–1608, <https://doi.org/10.1016/j.solener.2010.12.002>.
- [3] W. Li, R. Yang, D. Wang, CdTe solar cell performance under high-intensity light irradiance, Sol. Energy Mater. Sol. Cells 123 (2014) 249–254, <https://doi.org/10.1016/j.solmat.2014.01.021>.
- [4] A. Chirilă, S. Buecheler, F. Pianezzi, P. Bloesch, C. Gretener, A.R. Uhl, C. Fella, L. Kranz, J. Perrenoud, S. Seyrling, R. Verma, S. Nishiwaki, Y.E. Romanyuk, G. Bilger, A.N. Tiwari, Highly efficient Cu (In, Ga) Se 2 solar cells grown on flexible polymer films, Nat. Mater. 10 (11) (2011) 857–861, <https://doi.org/10.1038/nmat3122>.
- [5] S.M. Hubbard, C.D. Cress, C.G. Bailey, R.P. Raffaelle, S.G. Bailey, D.M. Wilt, Effect of strain compensation on quantum dot enhanced GaAs solar cells, Appl. Phys. Lett. 92 (12) (2008) 123512, <https://doi.org/10.1063/1.2903699>.
- [6] M.E. Ragoussi, T. Torres, New generation solar cells: concepts, trends and perspectives, Chem. Commun. 51 (19) (2015) 3957–3972, <https://doi.org/10.1039/C4CC0988A>.
- [7] T.R. Andersen, H.F. Dam, M. Hösel, M. Helgesen, J.E. Carlé, T.T. Larsen-Olsen, S. Gevorgyan, J.W. Andreasen, J. Adams, N. Li, F. Machui, G.D. Spyropoulos,

- T. Ameri, N. Lemaître, M. Legros, A. Scheel, D. Gaiser, K. Kreul, S. Berny, O. R. Lozman, S. Nordman, M. Välimäki, M. Vilkanen, R.R. Søndergaard, M. Jørgensen, C.J. Brabec, F.C. Krebs, Scalable, ambient atmosphere roll-to-roll manufacture of encapsulated large area, flexible organic tandem solar cell modules, *Energy Environ. Sci.* 7 (9) (2014) 2925, <https://doi.org/10.1039/C4EE01223B>.
- [8] M. Freitag, Q. Daniel, M. Pazoki, K. Sveinbjörnsson, J. Zhang, L. Sun, A. Hagfeldt, G. Boschloo, High-efficiency dye-sensitized solar cells with molecular copper phenanthroline as solid hole conductor, *Energy Environ. Sci.* 8 (9) (2015) 2634–2637, <https://doi.org/10.1039/C5EE01204J>.
- [9] Y. Xiao, J. Wu, J.-Y. Lin, G. Yue, J. Lin, M. Huang, Z. Lan, L. Fan, A dual function of high performance counter-electrode for stable quasi-solid-state dye-sensitized solar cells, *J. Power Sources* 241 (2013) 373–378, <https://doi.org/10.1016/j.jpowsour.2013.04.091>.
- [10] P. Roy, N.K. Sinha, S. Tiwari, A. Khare, A review on perovskite solar cells: Evolution of architecture, fabrication techniques, commercialization issues and status, *Sol. Energy* 198 (2020) 665–688, <https://doi.org/10.1016/j.solener.2020.01.080>.
- [11] Y. Wu, F. Xie, H. Chen, X. Yang, H. Su, M. Cai, Z. Zhou, T. Noda, L. Han, Thermally stable MAPbI₃ perovskite solar cells with efficiency of 19.19% and area over 1 cm² achieved by additive engineering, *Adv. Mater.* 29 (28) (2017) 1701073, <https://doi.org/10.1002/adma.v29.2810.1002/adma.201701073>.
- [12] B. O’regan, M. Grätzel, A low-cost, high-efficiency solar cell based on dye-sensitized colloidal TiO₂ films, *Nature* 353 (6346) (1991) 737–740, <https://doi.org/10.1038/353737a0>.
- [13] D. Dahlán, S.K.M. Saad, A.U. Berli, A. Bajili, A.A. Umar, Synthesis of two-dimensional nanowall of Cu-Doped TiO₂ and its application as photoanode in DSSCs, *Physica E* 91 (2017) 185–189, <https://doi.org/10.1016/j.physe.2017.05.003>.
- [14] S.K.M. Saad, A.A. Umar, M.Y.A. Rahman, M.M. Salleh, Porous Zn-doped TiO₂ nanowall photoanode: effect of Zn²⁺ concentration on the dye-sensitized solar cell performance, *Appl. Surf. Sci.* 353 (2015) 835–842, <https://doi.org/10.1016/j.apsusc.2015.06.181>.
- [15] X. Zhang, F. Liu, Q.L. Huang, G. Zhou, Z.S. Wang, Dye-sensitized W-doped TiO₂ solar cells with a tunable conduction band and suppressed charge recombination, *The journal of physical chemistry C* 115 (25) (2011) 12665–12671, <https://doi.org/10.1021/jp201853c>.
- [16] J.Y. Park, C.S. Kim, K. Okuyama, H.M. Lee, H.D. Jang, S.E. Lee, T.O. Kim, Copper and nitrogen doping on TiO₂ photoelectrodes and their functions in dye-sensitized solar cells, *J. Power Sources* 306 (2016) 764–771, <https://doi.org/10.1016/j.jpowsour.2015.12.087>.
- [17] B.-S. Kim, J.-Y. Park, C.-S. Kim, S.-B. Kim, D.-K. Song, H.-D. Jang, S.-E. Lee, T.-O. Kim, Zirconium oxide post-treatment for TiO₂ photoelectrodes in dye-sensitized solar cells, *Electrochim. Acta* 174 (2015) 502–507, <https://doi.org/10.1016/j.electacta.2015.06.022>.
- [18] S.N. Sadikin, M.Y.A. Rahman, A.A. Umar, M.M. Salleh, Effect of spin-coating cycle on the properties of TiO₂ thin film and performance of DSSC, *Int. J. Electrochem. Sci.* 12 (6) (2017) 5529–5538, <https://doi.org/10.20964/2017.06.5>.
- [19] A. El Haimeur, M. Makha, H. Bakkali, J.M. González-Leal, E. Blanco, M. Dominguez, Z.V. Voitenko, Enhanced performance of planar perovskite solar cells using dip-coated TiO₂ as electron transporting layer, *Sol. Energy* 195 (2020) 475–482, <https://doi.org/10.1016/j.solener.2019.11.094>.
- [20] A. Agrawal, S.A. Siddiqui, A. Soni, K. Khandelwal, G.D. Sharma, Performance analysis of TiO₂ based dye sensitized solar cell prepared by screen printing and doctor blade deposition techniques, *Sol. Energy* 226 (2021) 9–19, <https://doi.org/10.1016/j.solener.2021.08.001>.
- [21] C.S. Chou, Y.J. Lin, R.Y. Yang, K.H. Liu, Preparation of TiO₂/NiO composite particles and their applications in dye-sensitized solar cells, *Adv. Powder Technol.* 22 (1) (2011) 31–42, <https://doi.org/10.1016/j.apt.2010.03.003>.
- [22] M.S. Ahmad, A.K. Pandey, N. Abd Rahim, Advancements in the development of TiO₂ photoanodes and its fabrication methods for dye sensitized solar cell (DSSC) applications. A review, *Renew. Sustain. Energy Rev.* 77 (2017) 89–108, <https://doi.org/10.1016/j.rser.2017.03.129>.
- [23] H.Y. Hafeez, S.K. Lakhera, M. Ashokkumar, B. Neppolian, Ultrasound assisted synthesis of reduced graphene oxide (rGO) supported InVO₄-TiO₂ nanocomposite for efficient hydrogen production, *Ultranson. Sonochem.* 53 (2019) 1–10, <https://doi.org/10.1016/j.ultsonch.2018.12.009>.
- [24] B. Neppolian, Q. Wang, H. Jung, H. Choi, Ultrasonic-assisted sol-gel method of preparation of TiO₂ nano-particles: Characterization, properties and 4-chlorophenol removal application, *Ultranson. Sonochem.* 15 (4) (2008) 649–658, <https://doi.org/10.1016/j.ultsonch.2007.09.014>.
- [25] B. Neppolian, C. Wang, M. Ashokkumar, Sonochemically synthesized mono and bimetallic Au–Ag reduced graphene oxide based nanocomposites with enhanced catalytic activity, *Ultranson. Sonochem.* 21 (6) (2014) 1948–1953, <https://doi.org/10.1016/j.ultsonch.2014.02.006>.
- [26] Z.A. Zhou, Z. Xu, J.A. Finch, J.H. Masliyah, R.S. Chow, On the role of cavitation in particle collection in flotation—A critical review, II. Minerals engineering 22 (5) (2009) 419–433, <https://doi.org/10.1016/j.mineng.2008.12.010>.
- [27] P.N. Amaniampong, F. Jérôme, Catalysis under ultrasonic irradiation: a sound synergy, *Curr. Opin. Green Sustainable Chem.* 22 (2020) 7–12, <https://doi.org/10.1016/j.cogsc.2019.11.002>.
- [28] D. Panda, S. Manickam, Cavitation technology—The future of greener extraction method: A review on the extraction of natural products and process intensification mechanism and perspectives, *Applied Sciences* 9 (4) (2019) 766, <https://doi.org/10.3390/app9040766>.
- [29] P.I. Gouma, M.J. Mills, Anatase-to-rutile transformation in titania powders, *J. Am. Ceram. Soc.* 84 (3) (2001) 619–622, <https://doi.org/10.1111/j.1151-2916.2001.tb00709.x>.
- [30] D.G. Shchukin, E. Skorb, V. Belova, H. Möhwald, Ultrasonic cavitation at solid surfaces, *Adv. Mater.* 23 (17) (2011) 1922–1934.
- [31] X. Chen, L. Liu, Y.Y. Peter, S.S. Mao, Increasing solar absorption for photocatalysis with black hydrogenated titanium dioxide nanocrystals, *Science* 331 (6018) (2011) 746–750, <https://doi.org/10.1126/science.1200448>.
- [32] X. Pan, M.Q. Yang, X. Fu, N. Zhang, Y.J. Xu, Defective TiO₂ with oxygen vacancies: synthesis, properties and photocatalytic applications, *Nanoscale* 5 (9) (2013) 3601–3614, <https://doi.org/10.1039/c3nr00476g>.
- [33] S. Narakaew, The nano-TiO₂ synthesis using ultrasonic assisted sol-gel method and its photocatalytic degradation of methylene blue, *J. Ceram. Process. Res.* 18 (1) (2017) 36–40.
- [34] T. Xia, Y. Zhang, J. Murowchick, X. Chen, Vacuum-treated titanium dioxide nanocrystals: Optical properties, surface disorder, oxygen vacancy, and photocatalytic activities, *Catal. Today* 225 (2014) 2–9, <https://doi.org/10.1016/j.cattod.2013.08.026>.
- [35] M. Stucchi, C.L. Bianchi, C. Argirakis, V. Pifferi, B. Neppolian, G. Cerrato, D. C. Boffito, Ultrasound assisted synthesis of Ag-decorated TiO₂ active in visible light, *Ultranson. Sonochem.* 40 (2018) 282–288, <https://doi.org/10.1016/j.ultrsonch.2017.07.016>.
- [36] A. Katamipour, M. Farzam, I. Danaee, Effects of sonication on anticorrosive and mechanical properties of electrodeposited Ni-Zn-TiO₂ nanocomposite coatings, *Surf. Coat. Technol.* 254 (2014) 358–363, <https://doi.org/10.1016/j.surcoat.2014.06.043>.
- [37] K. Thamaphat, P. Limswan, B. Ngotawornchai, Phase characterization of TiO₂ powder by XRD and TEM, *Agric. Natl. Resour.* 42 (5) (2008) 357–361.
- [38] R. Yoshida, Y. Suzuki, S. Yoshikawa, Syntheses of TiO₂ (B) nanowires and TiO₂ anatase nanowires by hydrothermal and post-heat treatments, *J. Solid State Chem.* 178 (7) (2005) 2179–2185, <https://doi.org/10.1016/j.jssc.2005.04.025>.
- [39] M. Dhayal, J. Jun, H.B. Gu, K.H. Park, Surface chemistry and optical property of TiO₂ thin films treated by low-pressure plasma, *J. Solid State Chem.* 180 (10) (2007) 2696–2701, <https://doi.org/10.1016/j.jssc.2007.06.037>.
- [40] K. Safeen, V. Micheli, R. Bartali, G. Gottardi, A. Safeen, H. Ullah, N. Laidani, Synthesis of conductive and transparent Nb-doped TiO₂ films: role of the target material and sputtering gas composition, *Mater. Sci. Semicond. Process.* 66 (2017) 74–80, <https://doi.org/10.1016/j.mss.2017.04.012>.
- [41] M.Z. Atashbar, H.T. Sun, B. Gong, W. Włodarski, R. Lamb, XPS study of Nb-doped oxygen sensing TiO₂ thin films prepared by sol-gel method, *Thin Solid Films* 326 (1–2) (1998) 238–244, [https://doi.org/10.1016/S0040-6090\(98\)00534-3](https://doi.org/10.1016/S0040-6090(98)00534-3).
- [42] R. Wasielewski, J. Domaradzki, D. Wojciech, D. Kaczmarek, A. Borkowska, E. L. Prociow, A. Ciszewski, Surface characterization of TiO₂ thin films obtained by high-energy reactive magnetron sputtering, *Appl. Surf. Sci.* 254 (14) (2008) 4396–4400, <https://doi.org/10.1016/j.apsusc.2008.01.017>.
- [43] H. Perron, J. Vandenneborre, C. Domain, R. Drot, J. Roques, E. Simoni, J.-J. Ehrhardt, H. Catalette, Combined investigation of water sorption on TiO₂ rutile (1 1 0) single crystal face: XPS vs. periodic DFT, *Surf. Sci.* 601 (2) (2007) 518–527, <https://doi.org/10.1016/j.susc.2006.10.015>.
- [44] S.B. Kim, J.Y. Park, C.S. Kim, K. Okuyama, S.E. Lee, H.D. Jang, T.O. Kim, Effects of graphene in dye-sensitized solar cells based on nitrogen-doped TiO₂ composite, *J. Phys. Chem. C* 119 (29) (2015) 16552–16559, <https://doi.org/10.1021/acs.jpcc.5b02309>.
- [45] R. Mori, T. Ueta, K. Sakai, Y. Niida, Y. Koshiba, L.i. Lei, K. Nakamae, Y. Ueda, Organic solvent based TiO₂ dispersion paste for dye-sensitized solar cells prepared by industrial production level procedure, *J. Mater. Sci.* 46 (5) (2011) 1341–1350, <https://doi.org/10.1007/s10853-010-4925-2>.
- [46] M. Dhonde, K. Sahu, V.V.S. Murty, Cu-doped TiO₂ nanoparticles/graphene composites for efficient dye-sensitized solar cells, *Sol. Energy* 220 (2021) 418–424, <https://doi.org/10.1016/j.solener.2021.03.072>.
- [47] K. Sahu, M. Dhonde, V.V.S. Murty, Microwave-assisted hydrothermal synthesis of Cu-doped TiO₂ nanoparticles for efficient dye-sensitized solar cell with improved open-circuit voltage, *Int. J. Energy Res.* 45 (4) (2021) 5423–5432, <https://doi.org/10.1002/er.6169>.
- [48] M.J. Lee, J.Y. Park, C.S. Kim, K. Okuyama, S.E. Lee, T.O. Kim, Improvement of light scattering capacity in dye-sensitized solar cells by doping with SiO₂ nanoparticles, *J. Power Sources* 327 (2016) 96–103, <https://doi.org/10.1016/j.jpowsour.2016.07.032>.
- [49] J. Bisquert, Chemical capacitance of nanostructured semiconductors: its origin and significance for nanocomposite solar cells, *PCCP* 5 (24) (2003) 5360–5364, <https://doi.org/10.1039/B310907K>.
- [50] F. Fabregat-Santiago, G. García-Belmonte, I. Mora-Sero, J. Bisquert, Characterization of nanostructured hybrid and organic solar cells by impedance spectroscopy, *PCCP* 13 (20) (2011) 9083–9118, <https://doi.org/10.1039/C0CP02249G>.